Supporting Information

Sample et al. 10.1073/pnas.1001139107

SI Text

Notation. Separation of length scales is the basis of homogenization. We introduce here the small scale parameter ϵ as the ratio of the size of the reference cell to the size of the embryo:

$$\epsilon = \frac{l}{L}.$$

To establish notation, consider the cortical region of the entire embryo to be a bounded domain Ω. The geometric structure within Ω is obtained by the periodic repetition of the reference cell Y, where in this periodic geometry Ω_n^ϵ represents a nucleus, Γ^ϵ is the surface of a nucleus, and Ω_c^ϵ is the surrounding cytoplasm (Fig. 2*C* of the main text). The superscript ϵ indicates dependence on the period ϵL used to define the geometry. Species concentration and diffusivity are denoted $C_c^\epsilon(\mathbf{x},t)$ and D_c^ϵ in the cytoplasm, and $C_n^\epsilon(\mathbf{x},t)$ and D_n^ϵ in the nucleus. We assume that the nucleus and cytoplasm are isotropic, so that the diffusivities are scalar and constant. Because cytoplasmic and nuclear diffusivities are defined in their respective regions, the coefficients oscillate with period Y:

$$D_{c,n}^\epsilon(\mathbf{x}) = \begin{cases} D_{c,n} & \text{if } \mathbf{x} \in \Omega_{c,n}^\epsilon, \\ 0 & \text{otherwise.} \end{cases}$$

Nondimensionalization. The microscopic problem for concentration dynamics is given by

$$\frac{\partial C_c^\epsilon}{\partial t} = \nabla \cdot (D_c^\epsilon \nabla C_c^\epsilon), \qquad \mathbf{x} \in \Omega_c^\epsilon, \qquad \textbf{[S1]}$$

$$\frac{\partial C_n^\epsilon}{\partial t} = \nabla \cdot (D_n^\epsilon \nabla C_n^\epsilon), \qquad \mathbf{x} \in \Omega_n^\epsilon, \qquad \textbf{[S2]}$$

$$D_c^\epsilon \nabla C_c^\epsilon \cdot \mathbf{n} = D_n^\epsilon C_n^\epsilon \cdot \mathbf{n}, \qquad \mathbf{x} \in \Gamma^\epsilon, \qquad \textbf{[S3]}$$

$$D_c^\epsilon \nabla C_c^\epsilon \cdot \mathbf{n} = k_+ C_c^\epsilon - k_- C_n^\epsilon, \qquad \mathbf{x} \in \Gamma^\epsilon. \qquad \textbf{[S4]}$$

Here $\mathbf{n}$ is the outward normal to the boundary Γ^ϵ. Continuity of flux on the surface of the nucleus is imposed, and nuclear import and export are modeled as first-order reactions with interfacial mass transfer coefficients, k_+ and k_-. Their ratio $\kappa = k_+/k_-$ represents an equilibrium constant for nucleocytoplasmic shuttling. Equivalent descriptions have been used to describe interfacial transport between two immiscible fluids (1, 2) as well as interfacial transfer in porous media (1, 3).

To nondimensionalize the problem, we introduce the following dimensionless variables:

$$\tilde{\mathbf{y}} = \mathbf{x}/l, \qquad \tilde{t} = t/T, \qquad \tilde{C}_c^\epsilon = C_c^\epsilon / C_{\text{ref}}, \qquad \tilde{C}_n^\epsilon = C_n^\epsilon / C_{\text{ref}},$$

and dimensionless parameters:

$$\tilde{D}_c^\epsilon = \frac{T}{L^2} D_c^\epsilon, \qquad \tilde{D}_n^\epsilon = \frac{T}{L^2} D_n^\epsilon, \qquad \tilde{k}_- = \frac{T}{L} k_-, \qquad \kappa = k_+/k_-,$$

where T is the total duration of the last five nuclear cycles and C_{ref} is a reference concentration. These dimensionless numbers provide a measure for the relative influence of the system phenomena. By investigating orders of magnitude, we can determine the dominating mechanism that governs the concentration dynamics. Therefore, careful attention must be given to the dimensionless values because different types of macroscopic limit problems may result (3, 4).

The dimensionless numbers in this study are determined from the measurements for the diffusion constant of biologically inert molecules in the early embryo (5), cortical geometry (6), and nuclear cycle duration (7):

$$D_c = 15\ \mu\text{m}^2/\text{s}, \qquad L = 490\ \mu\text{m}, \qquad T = 7{,}200\ \text{s}. \qquad \textbf{[S5]}$$

The effective nuclear lifetime of Bicoid (Bcd) was measured to be about $\tau = 70$ s (6). Assuming Bcd is not degraded in the nucleus, we can compute the nuclear export rate using the average volume V_n and surface area S_n of a spherical nucleus at cycle 12 [average diameter ≈9 μm (6)]:

$$k_- = \frac{V_n}{S_n \tau} = 0.021\ \mu\text{m/s}. \qquad \textbf{[S6]}$$

According to Eqs. **S5** and **S6**, the following dimensionless parameters are calculated:

$$\tilde{D}_c^\epsilon = 0.45, \qquad \tilde{k}_- = 0.31.$$

To ensure proper scale separation such that the homogenization process works, the following condition must hold (3):

$$\frac{l^2}{T D_c^\epsilon} = \frac{\epsilon^2}{\tilde{D}_c^\epsilon} \sim O(\epsilon^2). \qquad \textbf{[S7]}$$

On the basis of our calculation for $\tilde{D}_c^\epsilon$, the condition of Eq. **S7** is met.

On account of lacking a measurement for the nuclear diffusion coefficient, we investigate possible regimes in which the diffusion coefficient may lie. We perform the homogenization analysis for different values of the exponent m in

$$\frac{D_n^\epsilon}{D_c^\epsilon} \sim O(\epsilon^m)$$

and compare the results. For $m < 2$, we find that the limit problems determined from homogenization are the same, assuming $\tilde{D}_c^\epsilon$, $\tilde{k}_-$, and $\kappa \sim O(1)$ (see ref. 4 for details). For ease of presentation, we let $m = 0$. Essentially, we are in a regime in which diffusion inside the nucleus does not affect morphogen gradient dynamics on the macroscale.

It is necessary to determine the strength of interfacial mass transfer relative to the diffusion process. In the literature (3), the Sherwood number is a dimensionless number relating the diffusivity of the interfacial barrier to the diffusivity within the component, similar to the Biot number in heat transfer. In our model, the Sherwood number is $\frac{lk_-}{D_c^\epsilon} = \epsilon \frac{\tilde{k}_-}{\tilde{D}_c^\epsilon} \sim O(\epsilon)$. On the basis of this calculation and experimental observation, we assume the system is in a regime of rapid nucleocytoplasmic kinetics (3). Thus, nuclear exchange occurs fast enough for cytoplasmic and nuclear concentrations to be in local equilibrium; κ represents the ratio of concentrations. Although a measurement for the nuclear import rate is unavailable, we can extract a value for κ from the concentration

profiles visualized in *Drosophila* embryos. Bicoid profiles are identified in embryos that have endogenous Bcd replaced with a fluorescent eGFP-Bcd fusion protein (6), from which it is determined that $\kappa \sim 5$.

The following dimensionless system is obtained:

$$\epsilon^2 \frac{\partial \tilde{C}_c^\epsilon}{\partial \tilde{t}} = \tilde{\nabla} \cdot (\tilde{D}_c^\epsilon \tilde{\nabla} \tilde{C}_c^\epsilon), \qquad \tilde{\mathbf{x}} \in \tilde{\Omega}_c^\epsilon, \tilde{t} \in (0,1), \qquad \textbf{[S8]}$$

$$\epsilon^2 \frac{\partial \tilde{C}_n^\epsilon}{\partial \tilde{t}} = \tilde{\nabla} \cdot (\tilde{D}_n^\epsilon \tilde{\nabla} \tilde{C}_n^\epsilon), \qquad \tilde{\mathbf{x}} \in \tilde{\Omega}_n^\epsilon, \tilde{t} \in (0,1), \qquad \textbf{[S9]}$$

$$\tilde{D}_c^\epsilon \tilde{\nabla} \tilde{C}_c^\epsilon \cdot \mathbf{n} = \tilde{D}_n^\epsilon \tilde{C}_n^\epsilon \cdot \mathbf{n}, \qquad \tilde{\mathbf{x}} \in \tilde{\Gamma}^\epsilon, \tilde{t} \in (0,1), \qquad \textbf{[S10]}$$

$$\tilde{D}_c^\epsilon \tilde{\nabla} \tilde{C}_c^\epsilon \cdot \mathbf{n} = \epsilon \tilde{k}_-(\kappa \tilde{C}_c^\epsilon - \tilde{C}_n^\epsilon), \qquad \tilde{\mathbf{x}} \in \tilde{\Gamma}^\epsilon, \tilde{t} \in (0,1). \qquad \textbf{[S11]}$$

Details of the Homogenization Approach. We describe here the approach for deriving an equivalent macroscopic description from the dimensionless microscopic system (Eqs. **S8–S11**). Tildes are dropped for convenience.

Asymptotic expansion. The syncytium is considered a multiscale system; we characterize it by two spatial variables, a local variable $\mathbf{y}$ and a global variable $\mathbf{x} = \epsilon \mathbf{y}$. The gradient operator is written as

$$\nabla \equiv \nabla_y + \epsilon \nabla_x,$$

where the subscripts indicate the partial derivatives with respect to $\mathbf{x}$ and $\mathbf{y}$. The two-scale asymptotic expansions for C_c^ϵ and C_n^ϵ have the form

$$C_c^\epsilon(\mathbf{x},\mathbf{y},t) = C_{c0}(\mathbf{x},\mathbf{y},t) + \epsilon C_{c1}(\mathbf{x},\mathbf{y},t) + \epsilon^2 C_{c2}(\mathbf{x},\mathbf{y},t) + \cdots,$$
$$C_n^\epsilon(\mathbf{x},\mathbf{y},t) = C_{n0}(\mathbf{x},\mathbf{y},t) + \epsilon C_{n1}(\mathbf{x},\mathbf{y},t) + \epsilon^2 C_{n2}(\mathbf{x},\mathbf{y},t) + \cdots,$$

where each term $C_j(\mathbf{x},\mathbf{y},t)$ is Y-periodic with respect to the microscopic variable. We begin the homogenization approach with an asymptotic analysis of the nondimensional system. First, the microscale problem is rewritten in terms of the asymptotic expansions. Then, by comparing the coefficients of different powers of ϵ, a cascade of equations for each term $C_j(\mathbf{x},\mathbf{y},t)$ is obtained. The boundary value problem in terms of ϵ is

$$\epsilon^2 \frac{\partial C_c^\epsilon}{\partial t} = (A_0^c + \epsilon^1 A_1^c + \epsilon^2 A_2^c) C_c^\epsilon, \qquad \mathbf{x} \in \Omega, \mathbf{y} \in \Omega_c^\epsilon, \qquad \textbf{[S12]}$$

$$\epsilon^2 \frac{\partial C_n^\epsilon}{\partial t} = (A_0^n + \epsilon^1 A_1^n + \epsilon^2 A_2^n) C_n^\epsilon, \qquad \mathbf{x} \in \Omega, \mathbf{y} \in \Omega_n^\epsilon, \qquad \textbf{[S13]}$$

$$D_c^\epsilon(\nabla_y + \epsilon \nabla_x) C_c^\epsilon \cdot \mathbf{n} = \epsilon k_-(\kappa C_c^\epsilon - C_n^\epsilon), \qquad \mathbf{x} \in \Omega, \mathbf{y} \in \Gamma^\epsilon, \qquad \textbf{[S14]}$$

$$D_n^\epsilon(\nabla_y + \epsilon \nabla_x) C_n^\epsilon \cdot \mathbf{n} = \epsilon k_-(\kappa C_c^\epsilon - C_n^\epsilon), \qquad \mathbf{x} \in \Omega, \mathbf{y} \in \Gamma^\epsilon, \qquad \textbf{[S15]}$$

where, for $i \in (c,n)$,

$$A_0^i = \nabla_y \cdot (D_i^\epsilon \nabla_y), \qquad A_1^i = \nabla_y \cdot (D_i^\epsilon \nabla_x) + \nabla_x \cdot (D_i^\epsilon \nabla_y),$$
$$A_2^i = D_i^\epsilon \nabla_x^2.$$

Lowest order problems. The next step of the multiscale expansion method is to solve the problems for the lowest power of ϵ. The problem for cytoplasmic concentration at $O(1)$ is

$$A_0^c C_{c0} = 0, \qquad D_c^\epsilon \nabla_y C_{c0} \cdot \mathbf{n} = 0.$$

Because C_{c0} is periodic in Y, it follows that the only solution is a function independent of the local variable, $C_{c0} = C_{c0}(\mathbf{x},t)$. By similar reasoning, the only solution to

$$A_0^n C_{n0} = 0, \qquad D_n^\epsilon \nabla_y C_{n0} \cdot \mathbf{n} = 0,$$

in the region Ω_n^ϵ, is a function independent of the local variable, $C_{n0} = C_{n0}(\mathbf{x},t)$. The functions $C_{c0}(\mathbf{x},t)$ and $C_{n0}(\mathbf{x},t)$ serve as the first-term approximations.

The reference cell problem. The multiple scales approach of homogenization yields a boundary value problem that must be solved in order to determine the effective diffusivity. This boundary value problem, commonly referred to as the *cell problem*, arises from solving Eqs. **S12–S15** at $O(\epsilon)$:

$$A_0^c C_{c1} + A_1^c C_{c0} = 0, \qquad \textbf{[S16]}$$

$$A_0^n C_{n1} + A_1^n C_{n0} = 0, \qquad \textbf{[S17]}$$

$$D_c^\epsilon(\nabla_y C_{c1} + \nabla_x C_{c0}) \cdot \mathbf{n} = k_-(\kappa C_{c0} - C_{n0}), \qquad \textbf{[S18]}$$

$$D_n^\epsilon(\nabla_y C_{n1} + \nabla_x C_{n0}) \cdot \mathbf{n} = k_-(\kappa C_{c0} - C_{n0}). \qquad \textbf{[S19]}$$

We have shown that both C_{c0} and C_{n0} are $\mathbf{y}$-independent. From the divergence theorem, the right-hand sides of Eqs. **S18** and **S19** are zero. Thus, $C_{n0} = \kappa C_{c0}$, which signifies that the cytoplasmic and nuclear concentrations are in local equilibrium.

Eqs. **S17** and **S19** reduce to

$$\nabla_y \cdot (D_n^\epsilon(\nabla_y C_{n1} + \nabla_x C_{n0})) = 0, \qquad D_n^\epsilon(\nabla_y C_{n1} + \nabla_x C_{n0}) \cdot \mathbf{n} = 0.$$

To solve this system, we define a function

$$\alpha(\mathbf{x},\mathbf{y},t) = C_{n1} + \mathbf{y} \cdot \nabla_x C_{n0} + \tilde{\alpha}(\mathbf{x},t),$$

that satisfies

$$\nabla_y \cdot (D_n^\epsilon \nabla_y \alpha) = 0, \qquad D_n^\epsilon \nabla_y \alpha \cdot \mathbf{n} = 0,$$

in the region Ω_n^ϵ. The solution, $\alpha(\mathbf{x},\mathbf{y},t) = 0$, generates the following equality:

$$D_n^\epsilon(\nabla_y C_{n1} + \nabla_x C_{n0}) = \mathbf{0}. \qquad \textbf{[S20]}$$

From Eqs. **S16** and **S18**:

$$\nabla_y \cdot (D_c^\epsilon(\nabla_y C_{c1} + \nabla_x C_{c0})) = 0, \qquad D_c^\epsilon(\nabla_y C_{c1} + \nabla_x C_{c0}) \cdot \mathbf{n} = 0.$$

A separation of variables for C_{c1} yields

$$C_{c1} = \mathbf{f}(\mathbf{y}) \cdot \nabla_x C_{c0} + \bar{C}_{c1}(\mathbf{x},t), \qquad \textbf{[S21]}$$

where $\bar{C}_{c1}(\mathbf{x},t)$ is an arbitrary function independent of the microscopic variable and $\mathbf{f}(\mathbf{y})$ is a correction to the homogenized solution $C_{c0}(\mathbf{x},t)$. The function f_k is the Y-periodic solution to the cell problem:

$$\nabla_y \cdot (D_c^\epsilon(\nabla_y f_k + \mathbf{e}_k)) = 0, \qquad \mathbf{y} \in \Omega_c^\epsilon, \qquad \textbf{[S22]}$$

$$D_c^\epsilon(\nabla_y f_k + \mathbf{e}_k) \cdot \mathbf{n} = 0, \qquad \mathbf{y} \in \Gamma^\epsilon. \qquad \textbf{[S23]}$$

The cell problems are solved numerically; details of the calculations are described below.

The homogenized equation. The third term in the expansion of cytoplasmic and nuclear concentrations must be considered in order to obtain a first-term approximation. The problem at $O(\epsilon^2)$ is

$$\frac{\partial C_{c0}}{\partial t} = A_0^c C_{c2} + A_1^c C_{c1} + A_2^c C_{c0}, \qquad \textbf{[S24]}$$

$$\frac{\partial C_{n0}}{\partial t} = A_0^n C_{n2} + A_1^n C_{n1} + A_2^n C_{n0}, \qquad \textbf{[S25]}$$

$$D_c^\epsilon(\nabla_y C_{c2} + \nabla_x C_{c1}) \cdot \mathbf{n} = k_-(\kappa C_{c1} - C_{n1}), \qquad \textbf{[S26]}$$

$$D_n^\epsilon(\nabla_y C_{n2} + \nabla_x C_{n1}) \cdot \mathbf{n} = k_-(\kappa C_{c1} - C_{n1}). \qquad \textbf{[S27]}$$

To obtain an equation for nuclear dynamics, we integrate Eq. **S25** on Ω_n^ϵ and apply Eqs. **S27** and **S20**:

$$|\Omega_n^\epsilon| \frac{\partial C_{n0}}{\partial t} = \int_{\Gamma^\epsilon} k_-(\kappa C_{c1} - C_{n1}) dS_y. \qquad \textbf{[S28]}$$

Next, we integrate Eq. **S24** on Ω_c^ϵ and apply Eqs. **S26** and **S21** and the periodicity condition to obtain an evolution equation for cytoplasmic concentration:

$$|\Omega_c^\epsilon| \frac{\partial C_{c0}}{\partial t} = \frac{\partial C_{c0}^2}{\partial x_j \partial x_k} \int_{\Omega_c^\epsilon} D_c \left(\frac{\partial f_k}{\partial y_j} + \delta_{jk} \right) dV_y - \int_{\Gamma^\epsilon} k_-(\kappa C_{c1} - C_{n1}) dS_y, \qquad \textbf{[S29]}$$

where δ_{jk} is the Kronecker delta function and summation notation is assumed. Because cytoplasmic and nuclear concentrations are in local equilibrium, Eqs. **S28** and **S29** yield a first-order approximation for cytoplasmic concentration:

$$(\phi + (1-\phi)\kappa) \frac{\partial C_{c0}}{\partial t} = \mathbf{D_G} \nabla_x^2 C_{c0}, \qquad \mathbf{x} \in \Omega.$$

The components of the effective diffusion tensor $\mathbf{D_G} = (D_{jk})_{j,k}$ are defined as

$$D_{jk} = \frac{1}{|Y|} \int_{\Omega_c^\epsilon} D_c \left(\frac{\partial f_k}{\partial y_j} + \delta_{jk} \right) dV_y.$$

In general, the tensor is symmetric and positive definite. The geometry of the cortical region of the early embryo, namely, a layer of symmetric inclusions between two reflective surfaces, generates a diffusion tensor with zero elements except for $D_{11} = D_{22}$. Therefore, the system pertaining to this paper yields a D_G that is scalar and, without loss of generality, is determined by the cell problem for f_1:

$$D_G = \frac{1}{|Y|} \int_{\Omega_c^\epsilon} D_c \left(\frac{\partial f_1}{\partial y_1} + 1 \right) dV_y.$$

Note in the main text we refer to the relative diffusivity, $G = D_G/D_c$.

Numerical Calculation of the Effective Diffusivity. In order to determine the effective diffusivity defined in Eq. **4** of the main text, the cell problem (Eqs. **S22** and **S23**) is solved using finite element methods with COMSOL Multiphysics (COMSOL, Inc.). The problem for f_1 simplifies to solving Laplace's equation in Ω_c^ϵ, with boundary condition

$$\nabla f_1 \cdot \mathbf{n} = \mathbf{e_1} \cdot \mathbf{n}$$

on the surface of the nucleus. The reference cell is modeled as a sphere inside a cuboid of variable size (Fig. 2*C* in the main text). Periodic boundary conditions on the lateral faces are imposed, as well as a reflective boundary condition on the top of the cuboid, the barrier between the embryo and the outside environment. We also impose a reflective boundary condition on the bottom of the cuboid, which we recognize as an assumption, because there is no well defined barrier between the periplasm and yolk. Each cell problem needs to be solved only once for a given geometric configuration.

As an test of our results using finite element methods, we solved the problem on a 201^3 grid with the successive overrelaxation method. Convergence was assumed when the solution changed by less than 10^{-4}% in one iteration. The results are nearly identical, with an error on the order of 10^{-3}. As a test of the homogenization approach for the case $\kappa = 0$, we performed Brownian-motion simulations of point particles to determine the diffusivity in the presence of spherical obstacles. The resulting effective diffusivities matched with the results obtained by homogenization (8).

Geometric Effects. In this section we address the sensitivity of our results on model geometry. It is observed that syncytial nuclei are arranged in a quasi-hexagonal lattice in the cortical region of the early embryo (9). For convenience, nuclei are aligned in a cubic lattice in our model. We check our results against simulations performed for nuclei arranged in a hexagonal lattice (8) and confirm that the configuration of inclusions has little influence on the diffusivity. This conclusion is consistent with previous studies (10, –12).

We also consider what happens to the diffusivity during cycle 14A when nuclei transform into objects shaped like rice grains. We investigate the effect of unidirectionally oriented inclusions on the diffusivity by simulating prolate spheroids with the major axis perpendicular to the plasma membrane. Consistent with other models, we conclude that the lateral diffusivity is lower for elongated nuclei than for nonelongated nuclei of the same volume (10, 11). Therefore, as nuclei lengthen during cycle 14A, a decreasing observed diffusion coefficient is expected (Fig. S1). We note, however, that the effect is not very significant (only ≈7% change). On the other hand, if the volume of a nucleus increases as it lengthens, elongation during late cycle 14A may play a more substantial role in decreasing the diffusivity. The insignificance of shape alone is apparent in Fig. S2, where the effective diffusivity for a range of parameters is plotted for both spherical nuclei and elongated nuclei.

Accuracy of the Maxwell Approximation. The relative effective diffusivity is a function of the geometry of the problem, namely, nuclear diameter, cortical thickness, the distance between the periodically arranged nuclei (size of the reference cell), and the distance between the nuclei and the outer membrane (position of a nucleus within the reference cell). We postulate that the portion of the effective diffusivity that depends only on geometry, G, can be described by Maxwell's formula, an expression that depends only on the volumetric space occupied by the nuclei. For a spherical nucleus inside a cuboidal cell, nuclear volume fraction is $1 - \phi = \frac{4/3\pi r^3}{l^2 h}$, which suggests that the effective diffusivity is independent of the precise location of the nuclei within the reference cell. It also implies that the effective diffusivity depends on a specific relationship of the geometric parameters, $\frac{r^3}{l^2 h}$, rather than on their exact values. We test the approximation of this

approximation by investigating the worse case: impenetrable nuclei, when $\kappa = 0$ and the relative effective diffusivity is $\frac{D_{\text{eff}}}{D_c} = \frac{G}{\phi}$. By scanning the range of physical parameters, we find that the maximum error is less than 6%. Accuracy is worst when the nuclei are very densely packed such that $l \approx 2r$ or when the cortical thickness is about the size of the nuclei, $h \approx 2r$. For the physical case when molecules can enter and exit the nuclei, we find that the error decreases with increasing κ. Specifically, for $\kappa = 1$, the error is less than 4%, and for $\kappa = 5$, the error is less than 2%. We therefore conclude that, for the physical range of parameters that describe the syncytial embryo, the geometric portion of the effective diffusivity can be accurately described by Maxwell's approximation.

Derivation of the Analytic Approximation. Maxwell's formula provides an exact approximation to the effective diffusivity when the reference cell is a cube. Although we have concluded that this historical formula provides a good estimate for our system, we seek an even better analytical approximation that accounts for the anisotropy of the cortical region. We do so by manipulating Maxwell's formula to derive an expression that depends not only on ϕ and κ but also on the detailed geometry of the syncytium, namely, nuclear radius and cortical thickness:

$$G = 1 - \frac{3(1-\phi)}{2 + \alpha(1-\phi)^{3/2}}, \qquad \textbf{[S30]}$$

where $\alpha = \sqrt{\frac{3}{4\pi}}\left(\frac{h}{r}\right)^{3/2}$. This estimate for the effective diffusivity is within 2% of our numerical results. Note that in the limit $\alpha \to 1/\sqrt{1-\phi}$, Maxwell's approximation is recovered. The expression is derived to provide an approximation for a noncubic reference cell, for the two cases of anisotropy: (*i*) The height of the cortex is greater than the length of the reference cell $h > l$, and (*ii*) the height of the cortex is smaller than the length of the reference cell $h < l$. For both cases, the analytic approximation is obtained by constructing a cube of length l around the spherical nucleus. We suppose that the effective diffusivity for this region follows Maxwell's formula:

$$\hat{G} = \frac{2\hat{\phi}}{3 - \hat{\phi}},$$

where

$$1 - \hat{\phi} = \frac{V_n}{\hat{V}_T} = \frac{V_n}{l^3}$$

is the volume fraction of the sphere inside the imagined cube. For the first case, the imagined cube is smaller than the reference cell. We assume molecules undergo free diffusion in the cytoplasmic region outside of the cube. The weighted average of the two diffusivities,

$$G = \frac{\hat{V}_T}{V_T}\hat{G} + \left(1 - \frac{\hat{V}_T}{V_T}\right),$$

yields Eq. **S30**. For the second case, the constructed cube is larger than the reference cell. We suppose that the effective diffusivity of the cube can be written in terms of the weighted average of the diffusivity of the reference cell and the (free) diffusivity in region outside of the reference cell:

$$\hat{G} = \frac{V_T}{\hat{V}_T}G + \left(1 - \frac{V_T}{\hat{V}_T}\right).$$

This also gives Eq. **S30**. Note in Fig. S2, the approximation breaks down when either the height of the cortical region or the length of the reference cell is about the same size as the diameter of the nucleus, presumably because we can no longer accurately capture molecular movement in an environment where inclusions are not well separated. The approximation, however, is still within 2% of our numerical results.

Three-Dimensional Analysis. We evaluate how well the homogenization technique approximates the real solution to the diffusion problem by comparing our homogenization results with 3-dimensional simulations of the problem. Spherical nuclei are arranged periodically along the length of the embryo. We take a section of the monolayer and impose the following boundary conditions: constant production at the anterior end of the embryo, zero flux at the posterior end, zero flux at the outer and inner membranes of the cortex, and periodic boundary conditions on the lateral faces. Solving the microscopic system, Eqs. **S1–S4**, with COMSOL Multiphysics (COMSOL) for a range of values for κ and ϕ, we find that the solution matches the homogenized solution with an error <1% (illustrated in Fig. 2*D* of the main text).

Details of Modeling the Bicoid Gradient. The 1-dimensional system of equations for the dynamics of Bicoid is given by

$$\frac{\partial C_c}{\partial t} = D_{\text{eff}}\frac{\partial^2 C_c}{\partial x^2} - \frac{(\phi k_c + \kappa(1-\phi)k_n)}{\phi + \kappa(1-\phi)}C_c + \frac{\phi}{\phi + \kappa(1-\phi)}j(x), \qquad \textbf{[S31]}$$

$$D_{\text{eff}}\frac{\partial C_c}{\partial x}\bigg|_{x=0} = 0, \qquad D_{\text{eff}}\frac{\partial C_c}{\partial x}\bigg|_{x=L} = 0. \qquad \textbf{[S32]}$$

The system is nondimensionalized using the following transformations: $z = x/L$, $\tau = t/T$, and $C(z,\tau) = D_c C(x,t)/QL$.

The effective diffusivity changes between nuclear cycles and is described by a piecewise constant function (Fig. S4). Gregor et al. (6) demonstrated that nuclear diameter increases during interphase, which explains the experimentally observed decrease in nuclear concentration during each cycle. Because we do not consider a dynamic nuclear diameter in this study, nuclear concentration predicted by the model actually increases during interphase (Fig. S5*D*). We note that a changing nuclear diameter can be included in the model by describing the effective diffusivity by a piecewise linear, time-dependent function.

Procedure to determine the width and stability of the gradient. The Bcd concentration profile is observed to have an exponential shape with a decay length between 10% and 20% of the embryo length (5). Using Matlab's fit function, we fit our numerical solution at the end of interphase i to an exponential curve: Ae^{-z/λ_i}. If $0.1 \le \bar{\lambda} \le 0.2$, then the gradient is considered to have the correct shape. We also ensure our numerical results are consistent with the nuclear-stability criterion: Gradients of nuclear Bcd are at least 10% accurate over the last five nuclear cycles between 10% and 50% of the embryo length (6). Stability is checked by computing the relative change of the gradient between two successive nuclear cycles: $g_{i,i-1}(z) = (N_i(z) - N_{i-1}(z))/N_{i-1}(z)$, where $0.1 \le z \le 0.5$ and $N_i(z)$ is the nondimensional nuclear concentration of cycle i. The function g is then averaged over both space and consecutive cycles. If the absolute value of the result is less than 0.1, the nuclear gradient is considered stable.

An example of gradient dynamics predicted by the model is shown in Fig. S5. The results are consistent with the shape, stability, and diffusivity determined by experiments. Examples of nuclear gradients that do not fit the criteria are shown in Fig. S6.

1. Hornung, U (1997) *Homogenization and Porous Media* (Springer, New York).
2. Brenner H, Leal LG (1978) Interfacial resistance to interphase mass transfer in quiescent two-phase systems. *AlChE J* 42:246–254.
3. Auriault JL, Lewandowska J (1997) Modelling of pollutant migration in porous media with interfacial transfer: Local equilibrium–non-equilibrium. *Mech Cohes-Frict Mat* 2:205–221.
4. Peter MA, Böhm M (2008) Different choices of scaling in homogenization of diffusion and interfacial exchange in a porous medium. *Math Method Appl Sci* 31:1257–1282.
5. Gregor T, Bialek W, de Ruyter van Steveninck RR, Tank DW, Wieschaus EF (2005) Diffusion and scaling during early embryonic pattern formation. *Proc Natl Acad Sci USA* 102:18403–18407.
6. Gregor T, Wieschaus EF, McGregor AP, Bialek W, Tank DW (2007) Stability and nuclear dynamics of the bicoid morphogen gradient. *Cell* 130:141–152.
7. Foe VE, Alberts BM (1983) Studies of nuclear and cytoplasmic behaviour during the five mitotic cycles that precede gastrulation in *Drosophila* embryogenesis. *J Cell Sci* 61:31–70.
8. Leffler AE (2009) Simulating diffusion in a heterogeneous, anisotropic medium: insights into the Bicoid gradient in *Drosophila melanogaster*. Senior thesis. Princeton University, New Jersey.
9. Warn RM, Magrath R (1983) F-actin distribution during the cellularization of the *Drosophila* embryo visualized with FL-phalloidin. *Expl Cell Res* 143:103–114.
10. El-Kareh AW, Braunstein SL, Secomb TW (1993) Effect of cell arrangement and interstitial volume fraction on the diffusivity of monoclonal antibodies in tissue. *Biophys J* 64:1638–1646.
11. Chang HC (1983) Effective diffusion and conduction in two-phase media: A unified approach. *AlChE J* 29:846–853.
12. Saez AE, Perfetti JC (1991) Prediction of effective diffusivities in porous media using spatially periodic models. *Trans Por Med* 6:143–157.

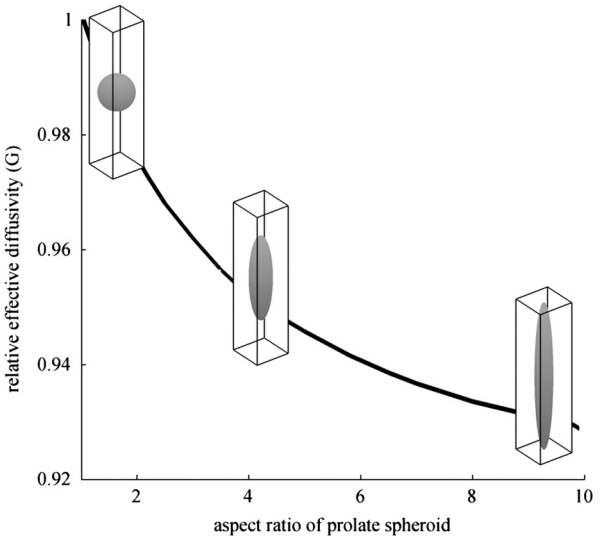

Fig. S1. The effective diffusivity depends weakly on nuclear shape for the geometric configuration of cycle 14. The portion of the relative effective diffusivity that characterizes volume exclusion effects is plotted as a function of the prolate spheroid's aspect ratio. Nuclear volume is fixed with a cortical thickness of 30 μm and a nuclear diameter of 6.5 μm.

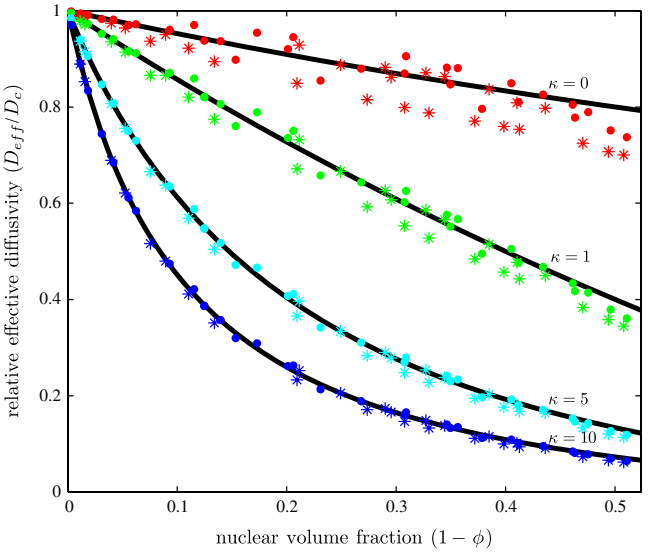

Fig. S2. The relative effective diffusivity plotted as a function of nuclear volume fraction for multiple values of the equilibrium constant. Each dot represents the effective diffusivity in the presence of spherical nuclei, for a particular set of geometric parameters as indicated in Fig. 3 of the main text. Each asterisk represents the effective diffusivity in the presence of spheroidal nuclei, where parameters are chosen from the following ranges: $r \in [0.7,5]$, $h \in [10,30]$, $l \in [3,24]$, and $\varepsilon \in [2,20]$, where ε is the ratio of the vertical radius to the horizontal radius. The solid lines are the analytical expression Eq. **S6** in the main text.

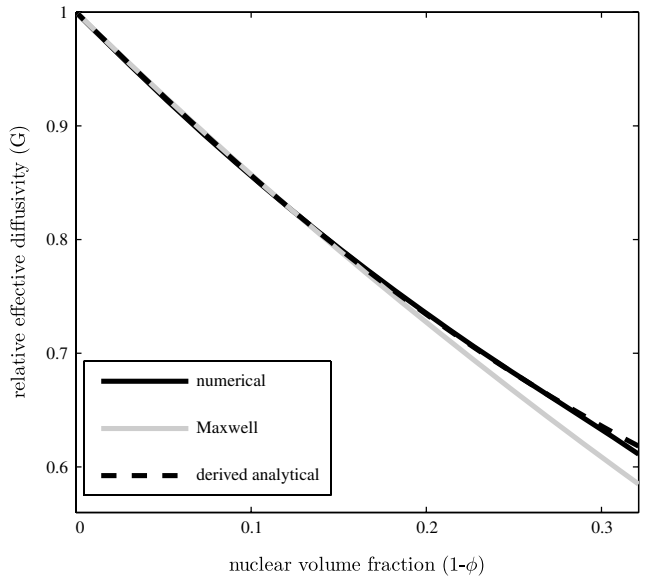

Fig. S3. The portion of the relative effective diffusivity that characterizes volume exclusion effects, *G*, is plotted as a function of nuclear volume fraction. *numerical* indicates that the function *G* is found computationally using finite element methods. *Maxwell* indicates that *G* is given by Maxwell's formula, and *derived analytical* refers to Eq. **30**.

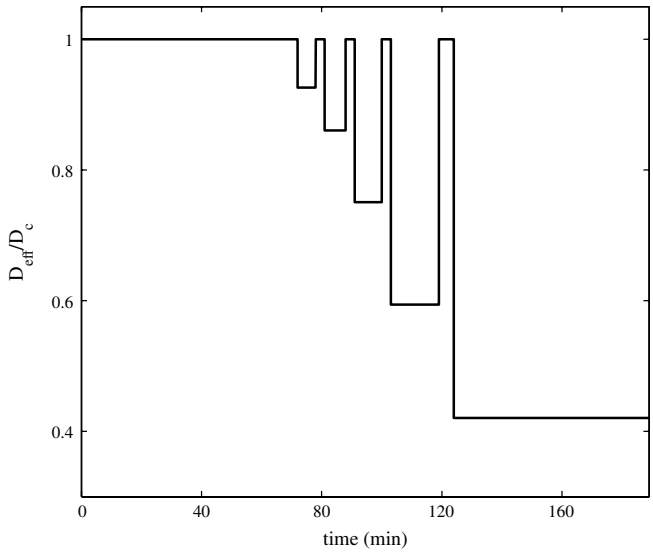

Fig. S4. The relative effective diffusivity as a function of time. During the interphase of each nuclear cycle, diffusivity is reduced, whereas free diffusion is restored during mitosis. Free diffusion is also assumed during the first 9 cycles because nuclear density is very low.

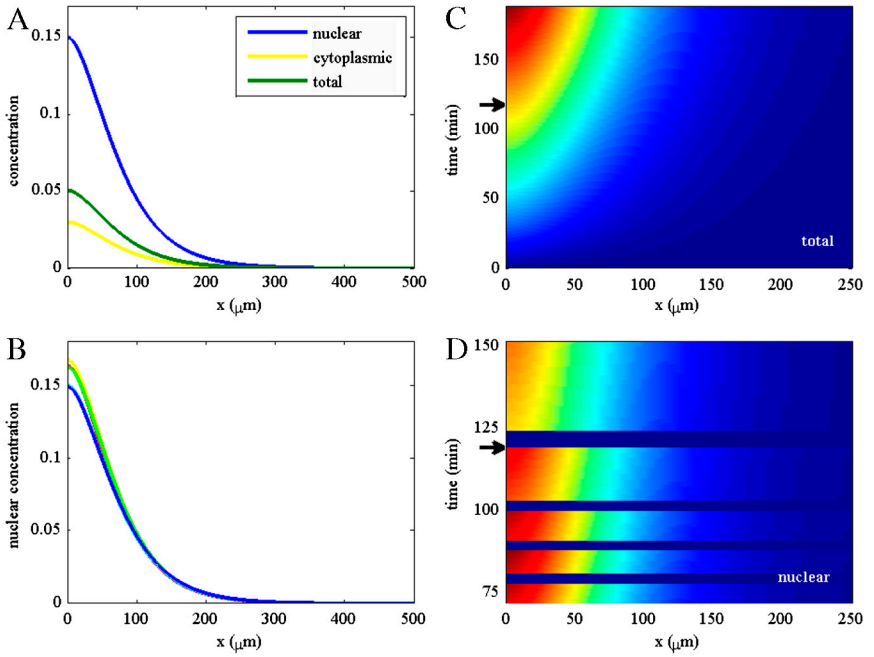

Fig. S5. The solution to the one-dimensional homogenized problem for Bicoid concentration that is consistent with the observed gradient dynamics. Here, $D_c = 0.3\ \mu m^2/s$, $k_c = 0$, $\lambda_s = 0.1$, and the other parameter values are indicated in Table S1. (*A*) Concentration profiles at the end of cycle 13 interphase. (*B*) The concentration of nuclear Bicoid at the end of interphase 10–14. For the chosen parameter values, the gradient of nuclear concentration, and consequently morphogen level per nucleus, is stable over the last five cycles. (*C*) Space-time plot of total concentration. The amplitude of the gradient increases as time progresses. (*D*) Space-time plot of nuclear concentration. Blue bands represent mitosis, the time when nuclear membranes are broken and nuclear concentration is zero. Arrows indicate the end of cycle 13 interphase.

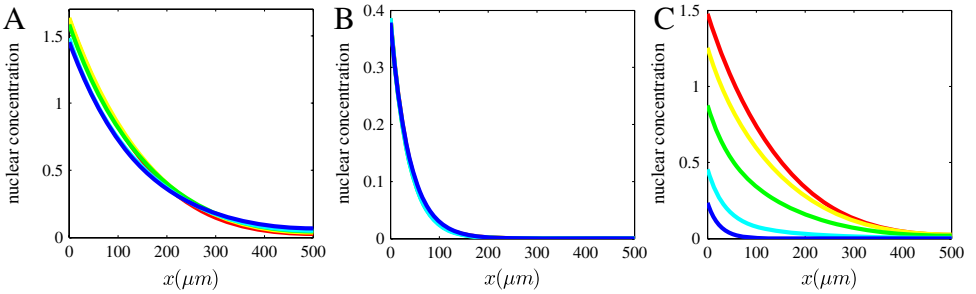

Fig. S6. Numerical solutions that are inconsistent with the observed gradient dynamics. The concentration of nuclear Bicoid at the end of interphase 10–14 are shown for $D_c = 5\ \mu m^2/s$, and $\lambda_s = 0$. (*A*) For $k_c = 0$ and $k_d = 0$, the gradient is too shallow. (*B*) For $k_c = 0.0033\ s^{-1}$ and $k_d = 0$, the gradient is too sharp. (*C*) For $k_c = 0$ and $k_d = 0.0033\ s^{-1}$, the nuclear gradient is unstable: Bcd levels per nucleus vary too much between cycles.

Table S1. Model parameters

Parameter	Value	Description
r	3.25 μm	Nuclear radius (average value at cycle 14); ref. 6
h	18 μm	Cortical thickness (averaged over cycles 10–14); ref. 6
L	500 μm	AP embryo length; ref. 6
H	180 μm	DV embryo length; ref. 6
T	72 min	Duration of cycles 1–9; ref. 7
T_{cyc}	9, 10, 12, 21, 65 min	Duration of cycles 10–14; ref. 7
T_{mit}	3, 3, 3, 5 min	Duration of mitosis for cycles 10–13; ref. 7
κ	5	Nuclear-cytoplasmic equilibrium constant; ref. 6
k_c	0–0.0033 s^{-1}	Cytoplasmic degradation rate
D_c	0–35 $\mu m^2/s$	Cytoplasmic diffusion constant
λ_s	0–100 μm	Characteristic length of the protein source